ACS OMEGA

Open Access

http://pubs.acs.org/journal/acsodf

Article

On the Versatility of the *sp*-, sp^2-, and sp^3-Hybridized Chalcogen-Bearing Molecules To Engage in Type I Chalcogen···Chalcogen Interactions: A Quantum Mechanical Investigation of Like···Like and Unlike Complexes

Mahmoud A. A. Ibrahim,* Rehab R. A. Saeed, Mohammed N. I. Shehata, Nayra A. M. Moussa, Mahmoud E. S. Soliman, Shahzeb Khan, Mohamed A. El-Tayeb, and Tamer Shoeib*

Cite This: *ACS Omega* 2024, 9, 44448−44456

Read Online

ACCESS | Metrics & More | Article Recommendations

ABSTRACT: The predilection of *sp*-, sp^2-, and sp^3-hybridized chalcogen-bearing molecules to engage in type I chalcogen···chalcogen interactions was comparatively unveiled in like···like/unlike CY···YC, YCY···YCY, and F_2Y···YF_2 (where Y = O, S, and Se) complexes, respectively. Upon the optimized monomers, a potential energy surface (PES) scan was conducted to pinpoint the most favorable complexes. The energetic findings unveiled the ability of the investigated systems to engage in the interactions under study with binding energy values ranging from −0.36 to −2.33 kcal/mol. Notably, binding energies were disclosed to align in the posterior sequence; sp^2- (i.e., YCY···YCY) > *sp*- (i.e., CY···YC) > sp^3- (i.e., F_2Y···YF_2) hybridized complexes, except the like···like oxygen-bearing complexes. Instead, the highest negative binding energy values were detected for the OCO···OCO followed by those of the F_2O···OF_2 and CO···OC complexes. Furthermore, the like···like selenium-bearing complexes demonstrated the most considerable binding energies compared to the other investigated complexes. Remarkably, the quantum theory of atoms in molecules and noncovalent interaction index analyses revealed the highly directional and closed-shell nature of the investigated chalcogen···chalcogen interactions. Symmetry adapted-perturbation theory findings outlined the dispersion forces as the commanding forces for all the studied complexes. These observations will provide convincing justifications for the nature of chalcogens within type I chalcogen···chalcogen interactions, leading to increased progress in various domains regarding drug design and materials science.

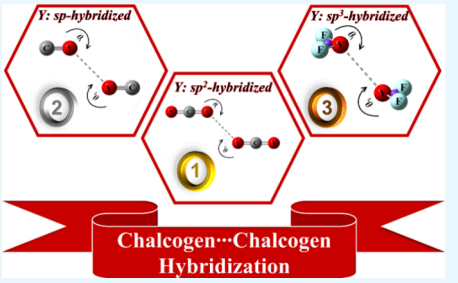

INTRODUCTION

Noncovalent interactions have been divulged as the primary basis for comprehending various chemical and biochemical processes.[1−7] Among the noncovalent interactions, hole interactions were announced as the most common member owing to their diverse applications, such as self-assembly,[8] ligand-acceptor interactions,[9,10] and anion recognition.[11] Principally, hole interactions were defined as an attractive interaction between a region with a low electron density over the entity of a molecule (i.e., hole) and a Lewis base.[12] Detailedly, the hole interactions were alterable based on the electron-accepting atom[13] relevant to Group IV−VIII elements and were classified as tetrel,[14−17] pnicogen,[18−23] chalcogen,[24−29] halogen,[30−33] and aerogen[34−37] bonds, respectively. Among hole interactions, many studies have focused on chalcogen bonding interactions because of their vital role in protein structure,[38] drug design,[39] and organic synthesis.[40] Chalcogen bonding interactions were first announced as an attractive interaction among the electron-deficient region of a Group IV element-bearing molecule and an electron-rich molecule.[28]

Along with chalcogen bonding interactions, chalcogen··· chalcogen interactions embraced a notable interest owing to its sundry applications in synthetic,[41,42] catalytic,[43,44] supramolecular,[45−47] biological,[48] and materials chemistry.[49,50] X-ray crystal structures also pinpointed that chalcogen··· chalcogen contact was commonly detected.[39,51−53]

Basically, several studies have demonstrated the occurrence of chalcogen···chalcogen interactions via favorable interactions between like and unlike chalcogenated complexes.[27,54−60] In the literature, chalcogen···chalcogen interactions within sp^2-hybridized-chalcogen bearing molecules YCY were assorted into four major classes, dubbed as type I, II, III, and IV chalcogen···chalcogen interactions (see Figure 1), parading that all the inspected complexes were driven by dispersion

Received: June 27, 2024
Revised: September 21, 2024
Accepted: September 30, 2024
Published: October 23, 2024

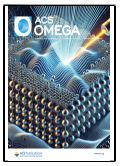

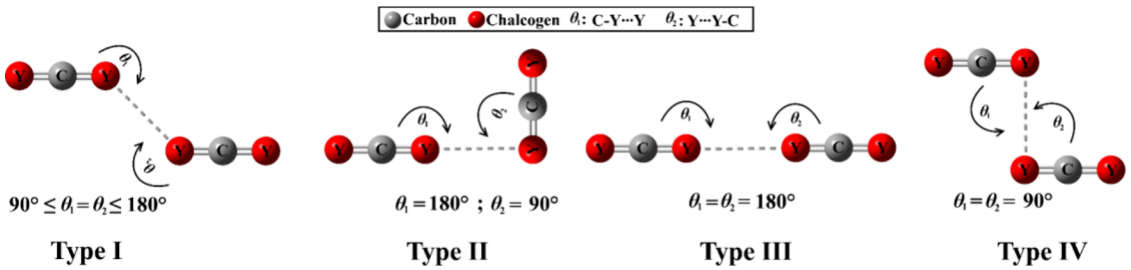

Figure 1. Descriptive representations of type I, II, III, and IV chalcogen···chalcogen interactions in Y═C═Y···Y═C═Y complexes where Y represents a chalcogen atom.

forces.[61] The same findings were denoted for the sp^3-hybridized-chalcogen-bearing molecules.[62,63]

However, there is still a paucity of studies demonstrating the nature and characteristics of chalcogen···chalcogen interactions within the sp^3-hybridized-chalcogen bearing molecules accompanied by no identification for these interactions within *sp*-hybridized-chalcogen bearing molecules.

Accordingly, a quantum mechanical investigation was herein established to unveil the potentiality of *sp*-hybridized chalcogen-bearing molecules to engage in type I chalcogen··· chalcogen interactions via like···like and unlike CY···YC complexes (where Y = O, S, and Se) (Figure 2). Afterward,

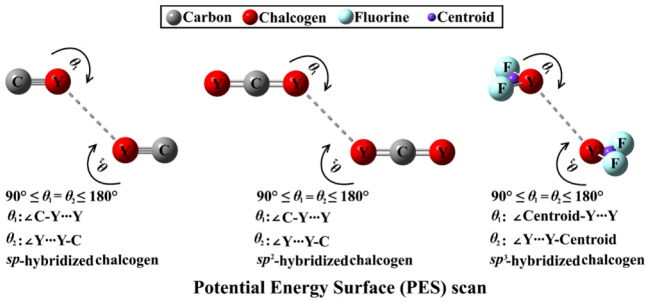

Figure 2. Descriptive representation of the PES of the type I chalcogen···chalcogen interactions within the like···like and unlike *sp*- (i.e., CY···CY), sp^2- (i.e., YCY···YCY), and sp^3- (i.e., $F_2Y\cdots YF_2$) hybridized complexes.

these interactions were compared with their analogues of sp^2- and sp^3- hybridized chalcogen-bearing molecules within the YCY···YCY and $F_2Y\cdots YF_2$ complexes, respectively. In this perspective, geometry optimization and electrostatic potential (EP) analysis were performed for the investigated chalcogen-bearing molecules. Upon the optimized monomers, a potential energy surface (PES) scan was conducted to pinpoint the most favorable complexes. Afterward, quantum theory of atoms in molecules (QTAIM), noncovalent interaction (NCI) index, and symmetry-adapted perturbation theory (SAPT) were performed for the most favorable complexes. The findings unearthed would be instructive for forthcoming applications pertinent to crystal engineering and materials research.

COMPUTATIONAL METHODS

A quantum mechanical investigation was herein executed to thoroughly unveil the ability of *sp*-, sp^2-, and sp^3-hybridized chalcogen-bearing molecules to engage in type I chalcogen··· chalcogen interactions in the fashion of like···like/unlike CY··· YC, YCY···YCY, and $F_2Y\cdots YF_2$ (where Y = O, S, and Se) complexes, respectively. First, all the inspected molecules were geometrically optimized employing the MP2/aug-cc-pVTZ level of theory.[64−66] The aug-cc-pVTZ(PP) basis set was adopted to account for the relativistic effects of the Se atom[67] and was obtained from the EMSL Basis Set Exchange Library.[68−70] Within the context of EP analysis, molecular electrostatic potential (MEP) maps were extracted to reveal the electron density distribution over the molecular skeleton for each molecule. In this vein, the 0.002 electron $bohr^{-3}$ contour of electron density was adopted due to its minute description of the EP on the molecular entity of the chemical systems, as previously recommended.[71,72]

Upon the optimized monomers, a PES scan was deliberated to comparatively evaluate the inclination of CY, YCY, and YF_2 molecules to participate in type I chalcogen···chalcogen interactions applying single point energy calculations. In the PES scan, a prolonged angular scope of $90° \le \theta_1 = \theta_2 \le 180°$ was invoked, where θ_1 and θ_2 represent, in successive, C−Y···Y and Y···Y−C for the *sp*-/sp^2-hybridized complexes, along with Centroid-Y···Y and Y···Y-Centroid for the sp^3-hybridized complexes (see Figure 2). PES scan was performed for the designed complexes at a distance scope starting from 2.5 to 5.0 Å with a step size of 0.1 Å. No vibrational frequency calculations were executed for the studied complexes, outlining the possibility that such structures might not be energetic minima. The binding energies (E_{bind}) were computed from the algebraic subtraction of the energy of the isolated monomers from the energy of the complex. For the assessed energetic quantities, the counterpoise corrected method was incorporated to eradicate basis set superposition error.[73] Benchmarking was afterward executed for all the considered complexes at the CCSD(T)/CBS level of theory as follows[74,75]:

$$E_{CCSD(T)/CBS} = \Delta E_{MP2/CBS} + \Delta E_{CCSD(T)} \quad (1)$$

where

$$\Delta E_{MP2/CBS} = (64E_{MP2/aug-cc-pVQZ(PP)} - 27E_{MP2/aug-cc-pVTZ(PP)})/37 \quad (2)$$

$$\Delta E_{CCSD(T)} = E_{CCSD(T)/aug-cc-pVDZ(PP)} - E_{MP2/aug-cc-pVDZ(PP)} \quad (3)$$

The nature of type I chalcogen···chalcogen interactions was manifested by employing the QTAIM[76] and NCI index[77] analyses. All calculations were carried out using Gaussian 09 software.[78] The EP, QTAIM, and NCI data were extracted utilizing Multiwfn 3.7 software.[79] The QTAIM and NCI schemes were generated utilizing the visual molecular dynamics program.[80] In order to unveil the physical nature of investigated interactions, SAPT analysis was fulfilled[81] at the SAPT2 level of truncation[81] with the help of PSI4 code.[82]

https://doi.org/10.1021/acsomega.4c05963
ACS Omega 2024, 9, 44448−44456

Using SAPT calculations, the total SAPT2 energy (E_{SAPT2}) was computed by summing its main physically meaningful energy quantities, namely electrostatic (E_{elst}), dispersion (E_{disp}), induction (E_{ind}), and exchange (E_{exch}) energies, as illustrated in eqs 4−8.[83] The attractive force percent ($E^{\%}_{attractive}$) was computed to determine to what extent each attractive components contribute to the total attractive forces ($E_{total\ attractive\ forces}$) through eq 9.

$$E_{SAPT2} = E_{elst} + E_{ind} + E_{disp} + E_{exch} \quad (4)$$

where:

$$E_{elst} = E^{(10)}_{elst} + E^{(12)}_{elst,r} \quad (5)$$

$$E_{ind} = E^{(20)}_{ind,r} + E^{(20)}_{exch-ind,r} + E^{(22)}_{ind} + E^{(22)}_{exch-ind} + \delta E^{(2)}_{HF,r} \quad (6)$$

$$E_{disp} = E^{(20)}_{disp} + E^{(20)}_{exch-disp} \quad (7)$$

$$E_{exch} = E^{(10)}_{exch} + E^{(11)}_{exch} + E^{(12)}_{exch} \quad (8)$$

$$E^{\%}_{attractive} = (E_{attractive\ component}/E_{total\ attractive\ force}) \times 100 \quad (9)$$

RESULTS AND DISCUSSION

EP Analysis. The EP analysis is considered as a well-established tool to effectively interpret the distribution of electron densities over the surface of a molecule.[84,85] The MEP maps of the inspected molecules are portrayed in Figure 3.

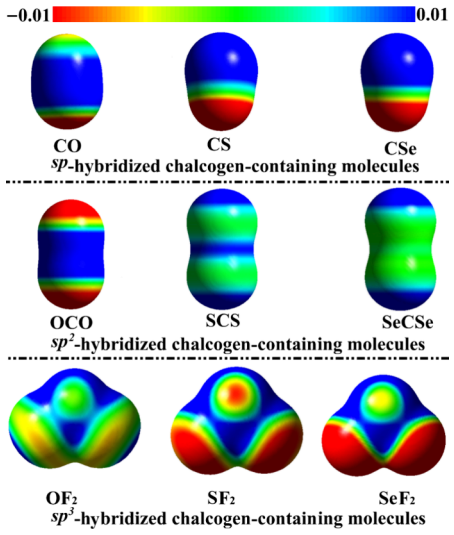

Figure 3. MEP maps of the investigated *sp*-, sp^2-, and sp^3-hybridized chalcogen-bearing molecules portrayed at the 0.002 au electron density contour.

From the delineated MEP maps in Figure 3, a variety of blue (i.e., electrophilic) and red (i.e., nucleophilic) sites were generally detected around the molecular surface of the examined systems. Regarding CY and YCY molecules, the EP analysis uncovered the most negative and positive EP over the outer surface relevant to the O and Se atoms, respectively. The molecular entity of all F_2Y molecules was noticed by the presence of both negative and positive EP. Overall, these findings reinforced the ability of *sp*- (i.e., CY), sp^2- (i.e., YCY), and sp^3- (i.e., F_2Y) hybridized chalcogen-bearing molecules to engage in a wide range of chalcogen···chalcogen interactions.

PES Scan. PES analysis was adopted to energetically elaborate the proclivity of the chemical systems to participate in noncovalent interactions. In this perspective, the optimized structures of the CY, YCY, and F_2Y monomers were modeled in the form of type I chalcogen···chalcogen interactions within the like···like and unlike *sp*- (i.e., CY···CY), sp^2- (i.e., YCY···YCY), and sp^3- (i.e., F_2Y···YF_2) hybridized complexes. Colored E_{bind} maps within an angular scope of $90° \le \theta_1 = \theta_2 \le 180°$ were visualized and are portrayed in Figure 4. Furthermore, MP2 energetic quantities were benchmarked at the CCSD(T)/CBS level of theory. The computed E_{bind} values at the most favorable complexation parameters are collected in Table 1.

As evident in Figure 4, the predilection of chalcogen-bearing molecules to engage in type I chalcogen···chalcogen interactions via like···like and unlike complexes was affirmed through the emerging negative E_{bind} values with higher preferability for selenium-bearing complexes. As numerical evidence from Table 1, E_{bind} values of the sp^3-hybridized complexes were−0.64,−0.50,−0.54,−0.55,−0.64, and−0.79 kcal/mol in the case of the F_2O···OF_2, F_2O···SF_2, F_2O···SeF_2, F_2S···SF_2, F_2S···SeF_2, and F_2Se···SeF_2 complexes, respectively. Conspicuously, the preferability of the studied complexes was noticed to augment relying on the following order: sp^3- (i.e., F_2Y···YF_2) < *sp*- (i.e., CY···YC) < sp^2- (i.e., YCY···YCY) hybridized complexes, except for the like···like oxygen-bearing complexes. For instance, E_{bind} were−0.79,−1.71, and−2.33 kcal/mol for F_2Se···SeF_2, CSe···SeC, and SeCSe···SeCSe complexes, respectively. Concerning the exceptional like···like oxygen-bearing complexes, significant E_{bind} values were observed for the sp^2- hybridized complexes followed by the sp^3- and *sp*-hybridized counterparts, respectively. Numerically, E_{bind} were−1.12,−0.64, and−0.36 kcal/mol for the OCO···OCO, F_2O···OF_2, and CO···OC complexes, respectively.

With respect to *sp*-hybridized complexes, binding energies of CO···OC complex were found to boost from E_{bind} value of −0.29 kcal/mol at $\theta_1 = \theta_2 = 180°$ until it reached its maximal value of −0.36 kcal/mol at $\theta_1 = \theta_2 = 132.5°$ and then faded again to −0.06 kcal/mol at θ_1 and $\theta_2 = 90°$. The preceding upshots were traced back to the preponderance of the negative belt···negative belt interactions at $\theta_1 = \theta_2 = 132.5°$. For the CO···SC and CO···SeC complexes, the escalating E_{bind} pattern was denoted by increasing θ_1 and θ_2 from 90° to 180°. This observation could be ascribed to the amelioration of the attractive forces between the negative clouds of the O atom and the maximal positive portions of the S/Se atoms. Numerically, the energetic quantities calculated for the CO···SeC complex were −0.25 and −0.55 kcal/mol at $\theta_1 = \theta_2 = 90°$ and 180°, respectively.

While MP2 energies of the CS···SC, CS···SeC, and CSe···SeC complexes were found with obvious elevation by dwindling θ_1 and θ_2 values from 180° to 90° and growing the atomic size of the interacting atoms. For instance, E_{bind} of CS···SC/CS···SeC/CSe···SeC complexes were 0.07/0.04/−0.01 and −1.28/−1.47/−1.71 kcal/mol at $\theta_1 = \theta_2 = 180°$ and 90°, respectively. In parallel, the same observations were exposed for the sp^2-hybridized complexes except for the OCO···OCO complex, where E_{bind} values were detected to augment at $\theta_1 = \theta_2 = 180°$ until it reached its maxima at 90°.

Turning to the sp^3-hybridized complexes, the energetic findings declared that the most nominal and copious E_{bind} values were recorded at $\theta_1 = \theta_2 = 180°$ and 90°, respectively.

https://doi.org/10.1021/acsomega.4c05963
ACS Omega 2024, 9, 44448−44456

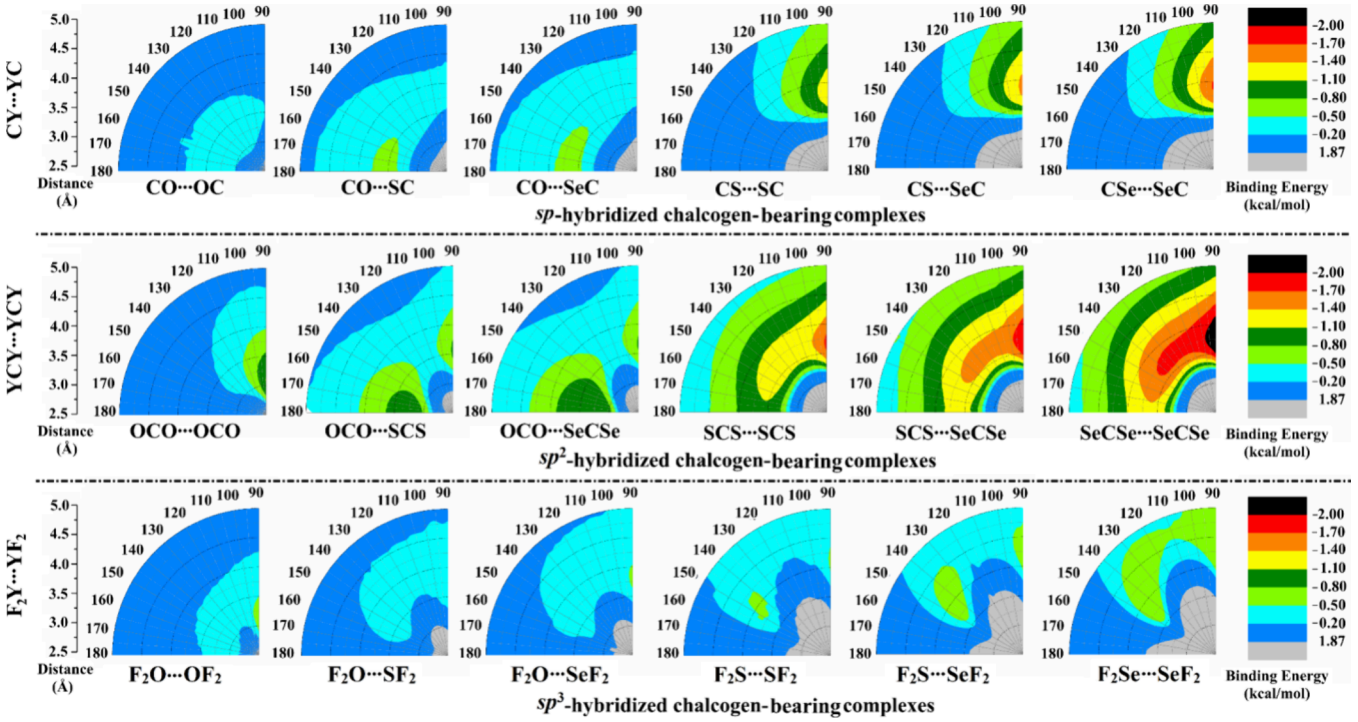

Figure 4. Colored E_{bind} maps of the investigated *sp*-, sp^2-, and sp^3-hybridized complexes.

Table 1. Calculated E_{bind} (in kcal/mol) of the CY···CY, YCY···YCY, and F_2Y···YF_2 complexes[a]

		complexation parameters[b]			binding energy	
complex	distance	θ_1	θ_2	Φ	$E_{MP2/aug-cc-pVTZ(pp)}$[c]	$E_{CCSD(T)/CBS}$
sp-hybridized complexes						
CO···OC	3.23	132.5°	132.5°	180°	−0.36	−0.23
CO···SC	3.53	180°	180°		−0.55	−0.45
CO···SeC	3.63	180°	180°		−0.55	−0.47
CS···SC	3.86	90°	90°		−1.28	−0.90
CS···SeC	3.90	90°	90°		−1.47	−1.00
CSe···SeC	3.93	90°	90°		−1.71	−1.10
sp^2-hybridized complexes						
OCO···OCO	3.09	90°	90°	180°	−1.12	−1.27
OCO···SCS	3.25	180°	180°		−0.99	−0.90
OCO···SeCSe	3.27	180°	180°		−1.23	−1.14
SCS···SCS	3.69	90°	90°		−1.76	−1.22
SCS···SeCSe	3.73	90°	90°		−2.00	−1.40
SeCSe···SeCSe	3.77	90°	90°		−2.33	−1.62
sp^3-hybridized complexes						
F_2O···OF_2	3.12	90°	90°	180°	−0.64	−0.67
F_2O···SF_2	3.69	90°	90°		−0.50	−0.57
F_2O···SeF_2	3.81	90°	90°		−0.54	−0.62
F_2S···SF_2	4.10	90°	90°		−0.55	−0.64
F_2S···SeF_2	3.95	90°	90°		−0.64	−0.76
F_2Se···SeF_2	4.32	90°	90°		−0.79	−0.97

[a]All distances and angles are in Å and degrees, respectively. [b]θ_1 and θ_2 refer to the ∠C−Y···Y and ∠Y···Y−C bond angles for *sp*/sp^2-hybridized complexes while ∠Centroid-Y···Y and ∠Y···Y-Centroid bond angles for sp^3-hybridized complexes, respectively. [c]The complexation parameters of most favorable complexes based on the E_{bind} maps in Figure 4.

Detailedly, the ascending order of the E_{bind} values was noted by decreasing θ_1 and θ_2 values from 180° to 145°. Afterward, E_{bind} values were diminished on going from $\theta_1 = \theta_2 = 145°$ to $\theta_1 = \theta_2 = 115°$ and then boosted again until reached their maxima at $\theta_1 = \theta_2 = 90°$. For instance, the energetic quantities of the F_2Se···SeF_2 complex were−0.24,−0.55,−0.37, and−0.79 kcal/mol at $\theta_1 = \theta_2 = 180°$, 145°, 115°, and 90°, respectively. Overall, the occurrence of the considered interactions could be interpreted as follows: (i) the attractive forces between the negative belt of the chalcogen atom and the positive portion of its analogue and (ii) the repulsive forces between the positive or negative clouds of the interacting chalcogen atoms. As compiled in Table 1, the calculated energetic features at the

https://doi.org/10.1021/acsomega.4c05963
ACS Omega 2024, 9, 44448−44456

CCSD(T)/CBS level of theory were generally in correspondence with the MP2 energy for all the explored complexes.

QTAIM Analysis. QTAIM analysis was carried out to elucidate the origin and nature of the interactions within the investigated complexes. Utilizing QTAIM, the BCPs and BPs were generated and are displayed in Figure 5. The computed values of ρ_b, $\nabla^2\rho_b$, H_b, and λ_2 at the BCPs within the studied complexes are listed in Table 2.

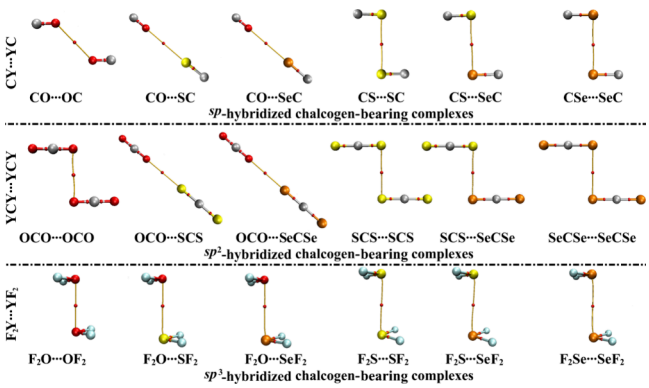

Figure 5. QTAIM scheme of the CY···YC, YCY···YCY, and $F_2Y\cdots YF_2$ complexes.

Table 2. ρ_b, $\nabla^2\rho_b$, H_b, and λ_2 (in au) of the CY···YC, YCY···YCY, and $F_2Y\cdots YF_2$ complexes

complex	ρ_b	$\nabla^2\rho_b$	H_b	λ_2
sp-hybridized complexes				
CO···OC	0.00311	0.01357	0.00081	−0.00238
CO···SC	0.00338	0.01375	0.00091	−0.00231
CO···SeC	0.00336	0.01259	0.00075	−0.00221
CS···SC	0.00424	0.01297	0.00078	−0.00227
CS···SeC	0.00464	0.01302	0.00068	−0.00244
CSe···SeC	0.00516	0.01309	0.00054	−0.00267
sp^2-hybridized complexes				
OCO···OCO	0.00601	0.02430	0.00126	−0.00455
OCO···SCS	0.00533	0.02462	0.00155	−0.00366
OCO···SeCSe	0.00593	0.02545	0.00142	−0.00393
SCS···SCS	0.00664	0.01865	0.00086	−0.00365
SCS···SeCSe	0.00722	0.01826	0.00066	−0.00386
SeCSe···SeCSe	0.00706	0.01663	0.00053	−0.00359
sp^3-hybridized complexes				
$F_2O\cdots OF_2$	0.00528	0.02169	0.00098	−0.00460
$F_2O\cdots SF_2$	0.00389	0.01215	0.00056	−0.00278
$F_2O\cdots SeF_2$	0.00375	0.01109	0.00048	−0.00258
$F_2S\cdots SF_2$	0.00397	0.01040	0.00061	−0.00248
$F_2S\cdots SeF_2$	0.00385	0.00960	0.00054	−0.00230
$F_2Se\cdots SeF_2$	0.00385	0.00926	0.00050	−0.00221

The QTAIM scheme in Figure 5 admitted the occurrence of the directional type I chalcogen···chalcogen interactions within all of the considered complexes via the emergence of a single BCP and BP without any clues for any secondary interactions. In addition, the ρ_b, $\nabla^2\rho_b$, and H_b were evidenced with positive numerical values, which in turn accentuated the closed-shell nature of all of the complexes under study (Table 2). Furthermore, negative values of λ_2 (i.e., $\lambda_2 < 0$) were disclosed for all complexes, announcing the bonding nature of their interactions. Notably, the numerical values of the topological parameters were detected to be in coincidence with energetic values, which were almost in correspondence with the MP2 consequences. As a case study, the H_b values were 0.00086, 0.00078, and 0.00061 au for SCS···SCS, CS···SC, and $F_2S\cdots SF_2$ complexes with MP2 values of −1.76, −1.28, and −0.55 kcal/mol, respectively.

NCI Analysis. NCI index was utilized to effectively provide a representative view into the nature of noncovalent interactions.[77] Within the employed NCI index, 3D NCI isosurfaces were generated for all of the studied complexes and are depicted in Figure 6.

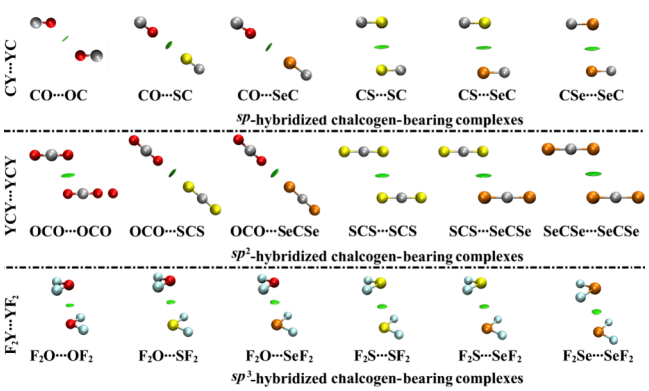

Figure 6. NCI plots of the CY···YC, YCY···YCY, and $F_2Y\cdots YF_2$ complexes.

As illustrated in Figure 6, the NCI plots manifested the ability of chalcogen-bearing molecules to form a type I chalcogen···chalcogen interaction via the presence of spherical green-coded isosurfaces with no observable indications for any secondary interactions. Apparently, the size of the circular isosurface area between the interacted species within the considered complexes was directly proportional to the energetic pattern resulting from the PES scan.

SAPT Analysis. SAPT analysis was accomplished to provide a precise explanation of the nature of noncovalent interactions from an energetic standpoint.[81] In turn, the total SAPT2 energies of the investigated complexes were dissected to identify the physically attractive and repulsive energetic components and are outlined in Figure 7 and Table 3.

As illustrated in Figure 7, the major preferable contributions to the total SAPT2 energies were traced back to E_{disp} for all the inspected complexes. In addition, the E_{elst} and E_{ind} forces were denoted with significant contributions to the total forces. It is worth mentioning that the negative values of the E_{elst} forces could be ascribed to the attractive interactions between the positive region of one chalcogen atom and the negative belt of the other chalcogen atom.[61] Polarization and charge transfer could also be a source of electrostatic stabilization between the two interacting chalcogen-bearing molecules, especially in the case of like···like chalcogen-bearing complexes.[86−88]

Positive numerical values of E_{exch} were remarked for all of the studied complexes, as listed in Table 3, announcing the repulsive contributions of E_{exch} to the energetic aspects. For example, the E_{elst}, E_{ind}, E_{disp}, and E_{exch} values of the CSe···SeC complex were −1.20, −0.33, −2.52, and 2.56 kcal/mol, respectively.

Generally, great compatibility was found between the MP2 energetic aspects and the negative values of the SAPT components. Illustratively, higher negative values of E_{elst}, E_{ind}, and E_{disp} were observed in the case of the sp^2-hybridized

https://doi.org/10.1021/acsomega.4c05963
ACS Omega 2024, 9, 44448−44456

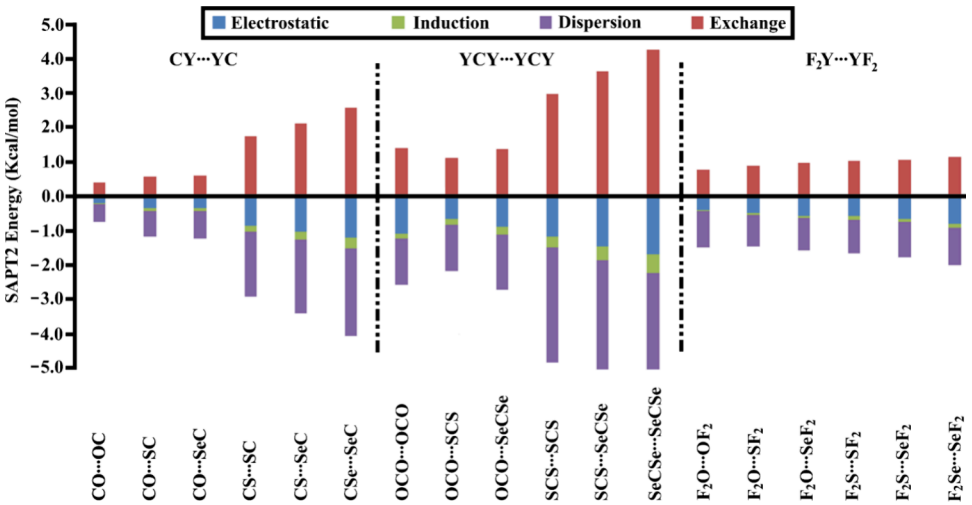

Figure 7. Bar chart of the four SAPT2 energy components of the CY···YC, YCY···YCY, and $F_2Y···YF_2$ complexes.

Table 3. E_{elst}, E_{ind}, E_{disp}, E_{exch}, E_{SAPT2}, and $\Delta\Delta E$ between E_{bind} and E_{SAPT2} of the CY···YC, YCY···YCY, and $F_2Y···YF_2$ complexes[a]

complex	E_{elst}	E_{ind}	E_{disp}	E_{exch}	E_{SAPT2}[b]	$\Delta\Delta E$[c]
sp-hybridized complexes						
CO···OC	−0.20	−0.03	−0.52	0.38	−0.37	0.01
CO···SC	−0.35	−0.08	−0.75	0.56	−0.62	0.07
CO···SeC	−0.35	−0.09	−0.79	0.58	−0.65	0.10
CS···SC	−0.87	−0.18	−1.87	1.72	−1.20	−0.08
CS···SeC	−1.03	−0.24	−2.16	2.10	−1.33	−0.14
CSe···SeC	−1.20	−0.33	−2.52	2.56	−1.50	−0.21
sp^2-hybridized complexes						
OCO···OCO	−1.09	−0.15	−1.35	1.40	−1.19	0.07
OCO···SCS	−0.67	−0.16	−1.36	1.10	−1.09	0.10
OCO···SeCSe	−0.90	−0.23	−1.58	1.37	−1.35	0.12
SCS···SCS	−1.19	−0.30	−3.34	2.98	−1.86	0.10
SCS···SeCSe	−1.46	−0.40	−3.83	3.63	−2.07	0.07
SeCSe···SeCSe	−1.70	−0.53	−4.38	4.26	−2.36	0.03
sp^3-hybridized complexes						
$F_2O···OF_2$	−0.40	−0.02	−1.08	0.77	−0.74	0.10
$F_2O···SF_2$	−0.50	−0.04	−0.92	0.87	−0.59	0.09
$F_2O···SeF_2$	−0.58	−0.06	−0.94	0.97	−0.61	0.07
$F_2S···SF_2$	−0.59	−0.09	−1.00	1.02	−0.66	0.11
$F_2S···SeF_2$	−0.67	−0.10	−1.02	1.05	−0.73	0.09
$F_2Se···SeF_2$	−0.82	−0.11	−1.07	1.13	−0.87	0.08

[a]All energies are given in kcal/mol. [b]$E_{SAPT2} = E_{disp} + E_{elst} + E_{ind} + E_{exch}$. [c]$\Delta\Delta E = E_{MP2/aug-cc-pVTZ(PP)} - E_{SAPT2}$.

complexes, followed by the *sp*- and sp^3-hybridized ones, with an exception for the like···like oxygen-bearing complexes. For instance, E_{elst}, E_{ind}, and E_{disp} were −1.20/−0.33/−2.52, −1.70/−0.53/−4.38, and −0.82/−0.11/−1.07 kcal/mol for like···like *sp*, sp^2, and sp^3selenium-bearing complexes, respectively.

The $\Delta\Delta E$ between E_{bind} and E_{SAPT2} was computed to verify the reliability of the implemented level in SAPT calculations. The tiny $\Delta\Delta E$ values were an indication of the accuracy of the selected SAPT level. Moreover, the attractive force percent ($E^{\%}_{attractive}$) of the individual SAPT2 components, including $E^{\%}_{disp}$, $E^{\%}_{elst}$, and $E^{\%}_{ind}$, were calculated and are graphed in Figure 8. As shown in Figure 8, for all the considered complexes, $E^{\%}_{disp}$ recorded about 52−72% of the total attractive forces, whereas $E^{\%}_{elst}$, and $E^{\%}_{ind}$ reached 25−42% and 1−8%, respectively.

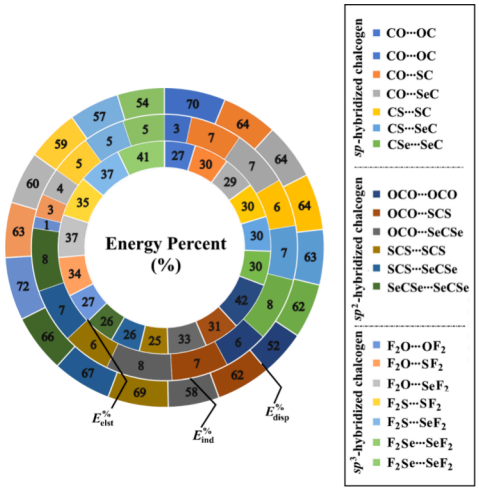

Figure 8. Doughnut graph demonstrating the $E^{\%}_{attractive}$ of each individual SAPT component of the CY···YC, YCY···YCY, and $F_2Y···YF_2$ complexes.

Illustratively, $E^{\%}_{disp}$, $E^{\%}_{elst}$, and $E^{\%}_{ind}$ were 62/66/54%, 30/26/41%, and 8/8/5% for like···like *sp*-, sp^2-, and sp^3-selenium-bearing complexes, respectively.

CONCLUSIONS

A quantum mechanical modeling was herein established to investigate the propensity of *sp*-, sp^2-, and sp^3-hybridized chalcogen-bearing molecules to engage in type I chalcogen···chalcogen interactions through like···like and unlike CY···YC, YCY···YCY, and $F_2Y···YF_2$ complexes (where Y = O, S, and Se), respectively. The selected monomers were first optimized and then subjected to a potential energy surface scan. The energetic upshots outlined that the E_{bind} were aligned in the posterior sequence; YCY···YCY > CY···YC > $F_2Y···YF_2$ hybridized complexes, regardless of the like···like in the case of Y = O. Instead, remarkable E_{bind} was detected for the OCO···OCO followed by the $F_2O···OF_2$ and CO···OC complexes, respectively. In succinct, the occurrence of the considered interactions could be interpreted as follows: (i) the attractive electrostatic forces between the negative belt of the chalcogen atom and positive portions of the corresponding chalcogen atom and (ii) the repulsive electrostatic forces

https://doi.org/10.1021/acsomega.4c05963
ACS Omega 2024, 9, 44448−44456

between the positive areas or negative clouds of the interacting chalcogen atoms. Conspicuously, the QTAIM and NCI analyses proclaimed the closed-shell nature of the scouted complexes and asserted the highly directional type I chalcogen···chalcogen interactions with no secondary interactions. The E_{SAPT2} upshots were generally consistent with the MP2 energies and showed that the studied interactions were dominated with E_{disp} for all the considered complexes. These observations would provide a clear perception of the comportment of the chalcogens, helping to achieve future improvement in crystal engineering and material science.

AUTHOR INFORMATION

Corresponding Authors

Mahmoud A. A. Ibrahim − *Computational Chemistry Laboratory, Chemistry Department, Faculty of Science, Minia University, Minia 61519, Egypt; School of Health Sciences, University of KwaZulu-Natal, Durban 4000, South Africa;* orcid.org/0000-0003-4819-2040; Email: m.ibrahim@compchem.net

Tamer Shoeib − *Department of Chemistry, The American University in Cairo, New Cairo 11835, Egypt;* orcid.org/0000-0003-3512-1593; Email: t.shoeib@aucegypt.edu

Authors

Rehab R. A. Saeed − *Computational Chemistry Laboratory, Chemistry Department, Faculty of Science, Minia University, Minia 61519, Egypt*

Mohammed N. I. Shehata − *Computational Chemistry Laboratory, Chemistry Department, Faculty of Science, Minia University, Minia 61519, Egypt;* orcid.org/0000-0002-3334-6070

Nayra A. M. Moussa − *Computational Chemistry Laboratory, Chemistry Department, Faculty of Science, Minia University, Minia 61519, Egypt; Basic and Clinical Medical Science Department, Faculty of Dentistry, Deraya University, New Minya 61768, Egypt;* orcid.org/0000-0003-3712-7710

Mahmoud E. S. Soliman − *Molecular Bio-Computation and Drug Design Research Laboratory, School of Health Sciences, University of KwaZulu-Natal, Durban 4000, South Africa;* orcid.org/0000-0002-8711-7783

Shahzeb Khan − *Centre for Pharmaceutical Engineering Science, Faculty of Life Science, School of Pharmacy and Medical Sciences, University of Bradford, Bradford BD7 1DP, U.K.;* orcid.org/0000-0002-3464-5435

Mohamed A. El-Tayeb − *Department of Botany and Microbiology, College of Science, King Saud University, Riyadh 11451, Saudi Arabia*

Complete contact information is available at: https://pubs.acs.org/10.1021/acsomega.4c05963

Author Contributions

M.A.A.I.: Conceptualization, Methodology, Software, Resources, Project Administration, Supervision, Writing—review and editing. R.R.A.S.: Data Curation, Formal Analysis, Investigation, Visualization, Writing—original draft. M.N.I.S.: Methodology, Investigation, Project Administration, Writing—review and editing. N.A.M.M.: Methodology, Investigation, Project Administration, Writing—review and editing. M.E.S.S.: Resources, Writing—review and editing. S.K.: Resources, Writing—review and editing. M.A.E.-T.: Visualization, Writing—review and editing. T.S.: Conceptualization, Resources, Methodology, Writing—review and editing.

Notes

The authors declare no competing financial interest.

ACKNOWLEDGMENTS

The authors extend their appreciation to the Researchers Supporting Project number (RSPD2024R678), King Saud University, Riyadh, Saudi Arabia, for funding this work. The computational work was completed with resources provided by the CompChem Lab (Minia University, Egypt, hpc.compchem.net), Center for High-Performance Computing (Cape Town, South Africa, http://www.chpc.ac.za), Bibliotheca Alexandrina (http://hpc.bibalex.org), and the American University in Cairo.

REFERENCES

(1) Jiang, S.; Zhang, L.; Cui, D.; Yao, Z.; Gao, B.; Lin, J.; Wei, D. The Important Role of Halogen Bond in Substrate Selectivity of Enzymatic Catalysis. *Sci. Rep.* **2016**, *6*, 34750−34756.

(2) Mahmudov, K. T.; Gurbanov, A. V.; Guseinov, F. I.; Guedes da Silva, M. F. C. Noncovalent interactions in metal complex catalysis. *Coord. Chem. Rev.* **2019**, *387*, 32−46.

(3) Mahler, H. C.; Friess, W.; Grauschopf, U.; Kiese, S. Protein aggregation: pathways, induction factors and analysis. *J. Pharm. Sci.* **2009**, *98*, 2909−2934.

(4) Whitesides, G. M.; Mathias, J. P.; Seto, C. T. Molecular self-assembly and nanochemistry: a chemical strategy for the synthesis of nanostructures. *Science* **1991**, *254*, 1312−1319.

(5) Huang, Z.; Qin, K.; Deng, G.; Wu, G.; Bai, Y.; Xu, J. F.; Wang, Z.; Yu, Z.; Scherman, O. A.; Zhang, X. Supramolecular chemistry of cucurbiturils: Tuning cooperativity with multiple noncovalent interactions from positive to negative. *Langmuir* **2016**, *32*, 12352−12360.

(6) Bartkowski, M.; Giordani, S. Supramolecular chemistry of carbon nano-onions. *Nanoscale* **2020**, *12*, 9352−9358.

(7) Ibrahim, M. A. A.; Shehata, M. N. I.; Moussa, N. A. M.; Hemia, R. R. A.; Abd Elhafez, H. S. M.; Abd El-Rahman, M. K.; Sayed, S. R. M.; Sidhom, P. A.; Dabbish, E.; Shoeib, T. Preferability of Molnupiravir, an anti-COVID-19 drug, toward purine nucleosides: A quantum mechanical study. *ACS Omega* **2023**, *8*, 27553−27565.

(8) Zeng, R.; Gong, Z.; Chen, L.; Yan, Q. Solution Self-Assembly of Chalcogen-Bonding Polymer Partners. *ACS Macro Lett.* **2020**, *9*, 1102−1107.

(9) Mani, D.; Arunan, E. The X-C···pi (X = F, Cl, Br, CN) carbon bond. *J. Phys. Chem. A* **2014**, *118*, 10081−10089.

(10) Mahmoudi, G.; Bauza, A.; Amini, M.; Molins, E.; Mague, J. T.; Frontera, A. On the importance of tetrel bonding interactions in lead(ii) complexes with (iso)nicotinohydrazide based ligands and several anions. *Dalton Trans.* **2016**, *45*, 10708−10716.

(11) Lim, J. Y. C.; Beer, P. D. Sigma-Hole Interactions in Anion Recognition. *Chem.* **2018**, *4*, 731−783.

(12) Tarannam, N.; Shukla, R.; Kozuch, S. Yet another perspective on hole interactions. *Phys. Chem. Chem. Phys.* **2021**, *23*, 19948−19963.

(13) Alkorta, I.; Elguero, J.; Frontera, A. Not only hydrogen bonds: Other noncovalent interactions. *Crystals* **2020**, *10*, 180−208.

(14) Scheiner, S. Origins and properties of the tetrel bond. *Phys. Chem. Chem. Phys.* **2021**, *23*, 5702−5717.

(15) Bhattarai, S.; Sutradhar, D.; Chandra, A. K. Strongly Bound pi-Hole Tetrel Bonded Complexes between H(2) SiO and Substituted Pyridines. Influence of Substituents. *ChemPhysChem* **2022**, *23*, No. e202200146.

(16) Ibrahim, M. A. A.; Shehata, M. N. I.; Rady, A. S. M.; Abuelliel, H. A. A.; Abd Elhafez, H. S. M.; Shawky, A. M.; Oraby, H. F.; Hasanin, T. H. A.; Soliman, M. E. S.; Moussa, N. A. M. Effects of Lewis basicity and acidity on sigma-hole interactions in carbon-bearing complexes: A comparative ab initio study. *Int. J. Mol. Sci.* **2022**, *23*, 13023.

https://doi.org/10.1021/acsomega.4c05963
ACS Omega 2024, 9, 44448−44456

(17) Ibrahim, M. A. A.; Mohamed, Y. A. M.; Abd Elhafez, H. S. M.; Shehata, M. N. I.; Soliman, M. E. S.; Ahmed, M. N.; Abd El-Mageed, H. R.; Moussa, N. A. M. R●-hole interactions of group IV-VII radical-containing molecules: A comparative study. *J. Mol. Graph. Model.* **2022**, *111*, No. 108097.
(18) Bauza, A.; Mooibroek, T. J.; Frontera, A. Sigma-hole opposite to a lone pair: Unconventional pnicogen bonding interactions between ZF3 (Z = N, P, As, and Sb) compounds and several donors. *ChemPhysChem* **2016**, *17*, 1608−1614.
(19) Feng, G.; Evangelisti, L.; Gasparini, N.; Caminati, W. On the Cl···N halogen bond: a rotational study of CF_3Cl···NH_3. *Chemistry* **2012**, *18*, 1364−1368.
(20) Murray, J. S.; Lane, P.; Politzer, P. A predicted new type of directional noncovalent interaction. *Int. J. Quantum Chem.* **2007**, *107*, 2286−2292.
(21) Scheiner, S. The pnicogen bond: its relation to hydrogen, halogen, and other noncovalent bonds. *Acc. Chem. Res.* **2013**, *46*, 280−288.
(22) Blanco, F.; Alkorta, I.; Rozas, I.; Solimannejad, M.; Elguero, J. A theoretical study of the interactions of NF(3) with neutral ambidentate electron donor and acceptor molecules. *Phys. Chem. Chem. Phys.* **2011**, *13*, 674−683.
(23) Alkorta, I.; Elguero, J.; Del Bene, J. E. Exploring the PX3:NCH and PX3:NH3 potential surfaces, with X = F, Cl, and Br. *Chem. Phys. Lett.* **2015**, *641*, 84−89.
(24) Bhattarai, S.; Sutradhar, D.; Huyskens, T. Z.; Chandra, A. K. Nature and Strength of the π-Hole Chalcogen Bonded Complexes between Substituted Pyridines and SO3 Molecule. *ChemistrySelect* **2021**, *6*, 7514−7524.
(25) Azofra, L. M.; Scheiner, S. Substituent Effects in the Noncovalent Bonding of SO(2) to Molecules Containing a Carbonyl Group. The Dominating Role of the Chalcogen Bond. *J. Phys. Chem. A* **2014**, *118*, 3835−3845.
(26) Varadwaj, P. R. Does Oxygen Feature Chalcogen Bonding? *Molecules* **2019**, *24*, 3166−3183.
(27) Wang, W.; Ji, B.; Zhang, Y. Chalcogen bond: A sister noncovalent bond to halogen bond. *J. Phys. Chem. A* **2009**, *113*, 8132−8135.
(28) Aakeroy, C. B.; Bryce, D. L.; Desiraju, G.; Frontera, A.; Legon, A. C.; Nicotra, F.; Rissanen, K.; Scheiner, S.; Terraneo, G.; Metrangolo, P.; Resnati, G. Definition of the chalcogen bond (IUPAC Recommendations 2019). *Pure Appl. Chem.* **2019**, *91*, 1889−1892.
(29) Ibrahim, M. A. A.; Saeed, R. R. A.; Shehata, M. N. I.; Moussa, N. A. M.; Tawfeek, A. M.; Ahmed, M. N.; Abd El-Rahman, M. K.; Shoeib, T. Sigma-hole and lone-pair-hole site-based interactions of seesaw tetravalent chalcogen-bearing molecules with Lewis bases. *ACS Omega* **2023**, *8*, 32828−32837.
(30) Zhou, F.; Liu, Y.; Wang, Z.; Lu, T.; Yang, Q.; Liu, Y.; Zheng, B. A new type of halogen bond involving multivalent astatine: an ab initio study. *Phys. Chem. Chem. Phys.* **2019**, *21*, 15310−15318.
(31) Bundhun, A.; Ramasami, P.; Murray, J. S.; Politzer, P. Trends in σ-hole strengths and interactions of F_3MX molecules (M = C, Si, Ge and X = F, Cl, Br, I). *J. Mol. Model.* **2013**, *19*, 2739−2746.
(32) Priimagi, A.; Cavallo, G.; Metrangolo, P.; Resnati, G. The halogen bond in the design of functional supramolecular materials: recent advances. *Acc. Chem. Res.* **2013**, *46*, 2686−2695.
(33) Desiraju, G. R.; Ho, P. S.; Kloo, L.; Legon, A. C.; Marquardt, R.; Metrangolo, P.; Politzer, P.; Resnati, G.; Rissanen, K. Definition of the halogen bond (IUPAC Recommendations 2013). *Pure Appl. Chem.* **2013**, *85*, 1711−1713.
(34) Bauza, A.; Frontera, A. π-Hole aerogen bonding interactions. *Phys. Chem. Chem. Phys.* **2015**, *17*, 24748−24753.
(35) Esrafili, M. D.; Asadollahi, S.; Vakili, M. Investigation of substituent effects in aerogen-bonding interaction between ZO_3(Z = Kr, Xe) and nitrogen bases. *Int. J. Quantum Chem.* **2016**, *116*, 1254−1260.
(36) Wang, R.; Liu, H.; Li, Q.; Scheiner, S. Xe···chalcogen aerogen bond. Effect of substituents and size of chalcogen atom. *Phys. Chem. Chem. Phys.* **2020**, *22*, 4115−4121.
(37) Ibrahim, M. A. A.; Shehata, M. N. I.; Abuelliel, H. A. A.; Moussa, N. A. M.; Sayed, S. R. M.; Ahmed, M. N.; Abd El-Rahman, M. K.; Dabbish, E.; Shoeib, T. Hole interactions of aerogen oxides with Lewis bases: an insight into σ-hole and lone-pair-hole interactions. *R. Soc. Open Sci.* **2023**, *10*, No. 231362.
(38) Iwaoka, M.; Isozumi, N. Hypervalent nonbonded interactions of a divalent sulfur atom. Implications in protein architecture and the functions. *Molecules* **2012**, *17*, 7266−7283.
(39) Beno, B. R.; Yeung, K. S.; Bartberger, M. D.; Pennington, L. D.; Meanwell, N. A. A Survey of the Role of Noncovalent Sulfur Interactions in Drug Design. *J. Med. Chem.* **2015**, *58*, 4383−4438.
(40) Rodríguez, S.; Kneeteman, M.; Izquierdo, J.; López, I.; González, F. V.; Peris, G. Diastereoselective synthesis of γ-hydroxy α,β-epoxyesters and their conversion into β-hydroxy α-sulfenyl γ-butyrolactones. *Tetrahedron* **2006**, *62*, 11112−11123.
(41) Shiina, I.; Nakata, K.; Ono, K.; Onda, Y. S.; Itagaki, M. Kinetic resolution of racemic alpha-arylalkanoic acids with achiral alcohols via the asymmetric esterification using carboxylic anhydrides and acyl-transfer catalysts. *J. Am. Chem. Soc.* **2010**, *132*, 11629−11641.
(42) Cox, P. A.; Leach, A. G.; Campbell, A. D.; Lloyd-Jones, G. C. Protodeboronation of Heteroaromatic, Vinyl, and Cyclopropyl Boronic Acids: pH-Rate Profiles, Autocatalysis, and Disproportionation. *J. Am. Chem. Soc.* **2016**, *138*, 9145−9157.
(43) Wang, W.; Zhu, H.; Feng, L.; Yu, Q.; Hao, J.; Zhu, R.; Wang, Y. Dual Chalcogen-Chalcogen Bonding Catalysis. *J. Am. Chem. Soc.* **2020**, *142*, 3117−3124.
(44) Benz, S.; Lopez-Andarias, J.; Mareda, J.; Sakai, N.; Matile, S. Catalysis with Chalcogen Bonds. *Angew. Chem., Int. Ed. Engl.* **2017**, *56*, 812−815.
(45) Lim, J. Y.; Marques, I.; Thompson, A. L.; Christensen, K. E.; Felix, V.; Beer, P. D. Chalcogen Bonding Macrocycles and [2]Rotaxanes for Anion Recognition. *J. Am. Chem. Soc.* **2017**, *139*, 3122−3133.
(46) Gleiter, R.; Werz, D. B.; Rausch, B. J. A world beyond hydrogen bonds? -Chalcogen-chalcogen interactions yielding tubular structures. *Chemistry* **2003**, *9*, 2676−2683.
(47) Robinson, S. W.; Mustoe, C. L.; White, N. G.; Brown, A.; Thompson, A. L.; Kennepohl, P.; Beer, P. D. Evidence for halogen bond covalency in acyclic and interlocked halogen-bonding receptor anion recognition. *J. Am. Chem. Soc.* **2015**, *137*, 499−507.
(48) Fick, R. J.; Kroner, G. M.; Nepal, B.; Magnani, R.; Horowitz, S.; Houtz, R. L.; Scheiner, S.; Trievel, R. C. Sulfur-Oxygen Chalcogen Bonding Mediates AdoMet Recognition in the Lysine Methyltransferase SET7/9. *ACS Chem. Biol.* **2016**, *11*, 748−754.
(49) Mahmudov, K. T.; Kopylovich, M. N.; Guedes da Silva, M. F. C.; Pombeiro, A. J. L. Chalcogen bonding in synthesis, catalysis and design of materials. *Dalton Trans.* **2017**, *46*, 10121−10138.
(50) Werz, D. B.; Gleiter, R.; Rominger, F. Nanotube formation favored by chalcogen-chalcogen interactions. *J. Am. Chem. Soc.* **2002**, *124*, 10638−10639.
(51) Shukla, R.; Chopra, D. Crystallographic and Theoretical Investigation on the Nature and Characteristics of Type I C═S···S═C Interactions. *Cryst. Growth Des.* **2016**, *16*, 6734−6742.
(52) Murray, J. S.; Lane, P.; Politzer, P. Simultaneous σ-hole and hydrogen bonding by sulfur- and selenium-containing heterocycles. *Int. J. Quantum Chem.* **2008**, *108*, 2770−2781.
(53) Murray, J. S.; Lane, P.; Clark, T.; Politzer, P. Sigma-hole bonding: molecules containing group VI atoms. *J. Mol. Model.* **2007**, *13*, 1033−1038.
(54) Sanz, P.; Yáñez, M.; Mó, O. Competition between X···H···Y Intramolecular Hydrogen Bonds and X····Y (X = O, S, and Y = Se, Te) Chalcogen−Chalcogen Interactions. *J. Phys. Chem. A* **2002**, *106*, 4661−4668.
(55) Sanz, P.; Mó, O.; Yáñez, M. Characterization of intramolecular hydrogen bonds and competitive chalcogen−chalcogen interactions

https://doi.org/10.1021/acsomega.4c05963
ACS Omega 2024, 9, 44448−44456

on the basis of the topology of the charge density. *Phys. Chem. Chem. Phys.* **2003**, *5*, 2942−2947.
(56) Mo, L.; Zeng, Y.; Li, X.; Meng, L. The enhancing effects of molecule X (X = PH2Cl, SHCl, ClCl) on chalcogen-chalcogen interactions in cyclic trimers Y···Y···X (Y = SHCl, SeHCl). *Int. J. Quantum Chem.* **2017**, *117*, No. e25354.
(57) Esrafili, M. D.; Saeidi, N.; Baneshi, M. M. Chalcogen−Chalcogen Interactions in Furan-YHX and Thiophene-YHX Complexes (X = F, Cl, Br; Y = S, Se): An Ab Initio Study. *Bull. Chem. Soc. Jpn.* **2015**, *88*, 1683−1692.
(58) Esrafili, M. D.; Mohammadian-Sabet, F. Homonuclear chalcogen−chalcogen bond interactions in complexes pairing YO3 and YHX molecules (Y = S, Se; X = H, Cl, Br, CCH, NC, OH, OCH3): Influence of substitution and cooperativity. *Int. J. Quantum Chem.* **2016**, *116*, 529−536.
(59) Trujillo, C.; Sánchez-Sanz, G.; Alkorta, I.; Elguero, J. Halogen, chalcogen and pnictogen interactions in (XNO2)2homodimers (X = F, Cl, Br, I). *New J. Chem.* **2015**, *39*, 6791−6802.
(60) Wang, R.; Lu, Y.; Xu, Z.; Liu, H. Triangular Interchalcogen Interactions: A Joint Crystallographic Data Analysis and Theoretical Study. *J. Phys. Chem. A* **2021**, *125*, 4173−4183.
(61) Ibrahim, M. A. A.; Shehata, M. N. I.; Soliman, M. E. S.; Moustafa, M. F.; El-Mageed, H. R. A.; Moussa, N. A. M. Unusual chalcogen···chalcogen interactions in like···like and unlike Y = C=Y··· Y = C=Y complexes (Y = O, S, and Se). *Phys. Chem. Chem. Phys.* **2022**, *24*, 3386−3399.
(62) Bleiholder, C.; Werz, D. B.; Koppel, H.; Gleiter, R. Theoretical investigations on chalcogen-chalcogen interactions: what makes these nonbonded interactions bonding? *J. Am. Chem. Soc.* **2006**, *128*, 2666−2674.
(63) Bleiholder, C.; Gleiter, R.; Werz, D. B.; Koppel, H. Theoretical investigations on heteronuclear chalcogen-chalcogen interactions: on the nature of weak bonds between chalcogen centers. *Inorg. Chem.* **2007**, *46*, 2249−2260.
(64) Møller, C.; Plesset, M. S. Note on an approximation treatment for many-electron systems. *Phys. Rev.* **1934**, *46*, 618−622.
(65) Kendall, R. A.; Dunning, T. H.; Harrison, R. J. Electron affinities of the first-row atoms revisited. Systematic basis sets and wave functions. *J. Chem. Phys.* **1992**, *96*, 6796−6806.
(66) Woon, D. E.; Dunning, T. H. Gaussian basis sets for use in correlated molecular calculations. III. The atoms aluminum through argon. *J. Chem. Phys.* **1993**, *98*, 1358−1371.
(67) Peterson, K. A.; Figgen, D.; Goll, E.; Stoll, H.; Dolg, M. Systematically convergent basis sets with relativistic pseudopotentials. II. Small-core pseudopotentials and correlation consistent basis sets for the post-d group 16−18 elements. *J. Chem. Phys.* **2003**, *119*, 11113−11123.
(68) Feller, D. The role of databases in support of computational chemistry calculations. *J. Comput. Chem.* **1996**, *17*, 1571−1586.
(69) Schuchardt, K. L.; Didier, B. T.; Elsethagen, T.; Sun, L.; Gurumoorthi, V.; Chase, J.; Li, J.; Windus, T. L. Basis set exchange: A community database for computational sciences. *J. Chem. Inf. Model.* **2007**, *47*, 1045−1052.
(70) Pritchard, B. P.; Altarawy, D.; Didier, B.; Gibson, T. D.; Windus, T. L. New basis set exchange: An open, up-to-date resource for the molecular sciences community. *J. Chem. Inf. Model.* **2019**, *59*, 4814−4820.
(71) Varadwaj, P. R.; Varadwaj, A.; Marques, H. M. Halogen bonding: A halogen-centered noncovalent interaction yet to be understood. *Inorganics* **2019**, *7*, 40−102.
(72) Ibrahim, M. A. A. Molecular mechanical perspective on halogen bonding. *J. Mol. Model.* **2012**, *18*, 4625−4638.
(73) Boys, S. F.; Bernardi, F. The calculation of small molecular interactions by the differences of separate total energies. Some procedures with reduced errors. *Mol. Phys.* **1970**, *19*, 553−566.
(74) Mishra, B. K.; Karthikeyan, S.; Ramanathan, V. Tuning the C-H···Pi interaction by different substitutions in benzene-acetylene complexes. *J. Chem. Theory Comput.* **2012**, *8*, 1935−1942.
(75) Helgaker, T.; Klopper, W.; Koch, H.; Noga, J. Basis-set convergence of correlated calculations on water. *J. Chem. Phys.* **1997**, *106*, 9639−9646.
(76) Bader, R. F. W. Atoms in molecules. *Acc. Chem. Res.* **1985**, *18*, 9−15.
(77) Johnson, E. R.; Keinan, S.; Mori-Sanchez, P.; Contreras-Garcia, J.; Cohen, A. J.; Yang, W. Revealing noncovalent interactions. *J. Am. Chem. Soc.* **2010**, *132*, 6498−6506.
(78) Frisch, M. J.; Trucks, G. W.; Schlegel, H. B.; Scuseria, G. E.; Robb, M. A.; Cheeseman, J. R.; Scalmani, G.; Barone, V.; Mennucci, B.; Petersson, G. A.; Nakatsuji, H.; Caricato, M.; Li, X.; Hratchian, H. P.; Izmaylov, A. F.; Bloino, J.; Zheng, G.; Sonnenberg, J. L.; Hada, M.; Ehara, M.; Toyota, K.; Fukuda, R.; Hasegawa, J.; Ishida, M.; Nakajima, T.; Honda, Y.; Kitao, O.; Nakai, H.; Vreven, T.; Montgomery, J. A.; Peralta, J. E.; Ogliaro, F.; Bearpark, M.; Heyd, J. J.; Brothers, E.; Kudin, K. N.; Staroverov, V. N.; Kobayashi, R.; Normand, J.; Raghavachari, K.; Rendell, A.; Burant, J. C.; Iyengar, S. S.; Tomasi, J.; Cossi, M.; Rega, N.; Millam, J. M.; Klene, M.; Knox, J. E.; Cross, J. B.; Bakken, V.; Adamo, C.; Jaramillo, J.; Gomperts, R.; Stratmann, R. E.; Yazyev, O.; Austin, A. J.; Cammi, R.; Pomelli, C.; Ochterski, J. W.; Martin, R. L.; Morokuma, K.; Zakrzewski, V. G.; Voth, G. A.; Salvador, P.; Dannenberg, J. J.; Dapprich, S.; Daniels, A. D.; Farkas, Ö.; Foresman, J. B.; Ortiz, J. V.; Cioslowski, J.; Fox, D. J. *Gaussian 09, Revision E01*; Gaussian Inc.: Wallingford CT, USA, 2009.
(79) Lu, T.; Chen, F. Multiwfn: a multifunctional wavefunction analyzer. *J. Comput. Chem.* **2012**, *33*, 580−592.
(80) Humphrey, W.; Dalke, A.; Schulten, K. VMD: Visual molecular dynamics. *J. Mol. Graph.* **1996**, *14*, 33−38.
(81) Hohenstein, E. G.; Sherrill, C. D. Density fitting and Cholesky decomposition approximations in symmetry-adapted perturbation theory: Implementation and application to probe the nature of pi-pi interactions in linear acenes. *J. Chem. Phys.* **2010**, *132*, 184111−184120.
(82) Turney, J. M.; Simmonett, A. C.; Parrish, R. M.; Hohenstein, E. G.; Evangelista, F. A.; Fermann, J. T.; Mintz, B. J.; Burns, L. A.; Wilke, J. J.; Abrams, M. L.; Russ, N. J.; Leininger, M. L.; Janssen, C. L.; Seidl, E. T.; Allen, W. D.; Schaefer, H. F.; King, R. A.; Valeev, E. F.; Sherrill, C. D.; Crawford, T. D. PSI4: An open-source ab initio electronic structure program. *Wiley Interdiscip. Rev. Comput. Mol. Sci.* **2012**, *2*, 556−565.
(83) Parker, T. M.; Burns, L. A.; Parrish, R. M.; Ryno, A. G.; Sherrill, C. D. Levels of symmetry adapted perturbation theory (SAPT). I. Efficiency and performance for interaction energies. *J. Chem. Phys.* **2014**, *140*, No. 094106.
(84) Weiner, P. K.; Langridge, R.; Blaney, J. M.; Schaefer, R.; Kollman, P. A. Electrostatic potential molecular surfaces. *Proc. Natl. Acad. Sci. U.S.A.* **1982**, *79*, 3754−3758.
(85) Murray, J. S.; Politzer, P. The electrostatic potential: An overview. *Wiley Interdiscip. Rev. Comput. Mol. Sci.* **2011**, *1*, 153−163.
(86) Ibrahim, M. A. A.; Saeed, R. R. A.; Shehata, M. N. I.; Ahmed, M. N.; Shawky, A. M.; Khowdiary, M. M.; Elkaeed, E. B.; Soliman, M. E. S.; Moussa, N. A. M. Type I−IV halogen···halogen interactions: A comparative theoretical study in halobenzene···halobenzene homodimers. *Int. J. Mol. Sci.* **2022**, *23*, 3114.
(87) Varadwaj, P.; Varadwaj, A.; Marques, H.; Yamashita, K. Can combined electrostatic and polarization effects alone explain the F···F negative-negative bonding in simple fluoro-substituted benzene derivatives? A first-principles perspective. *Computation* **2018**, *6*, 51−84.
(88) Mo, Y.; Danovich, D.; Shaik, S. The roles of charge transfer and polarization in non-covalent interactions: a perspective from ab initio valence bond methods. *J. Mol. Model.* **2022**, *28*, 274.

https://doi.org/10.1021/acsomega.4c05963
ACS Omega 2024, 9, 44448−44456